Validating EEG source imaging using intracranial electrical stimulation

Kanjana Unnwongse[1,*], Stefan Rampp[2,3,*], Tim Wehner[1], Annika Kowoll[1], Yaroslav Parpaley[4], Marec von Lehe[4], Benjamin Lanfer[1], Mateusz Rusiniak[5], Carsten Wolters[6,7], Jörg Wellmer[1]

[*]**Kanjana Unnwongse and Stefan Rampp contributed equally to this work.**

Author affiliations:

1 Ruhr-Epileptology, Department of Neurology, University Hospital Knappschaftskrankenhaus, Ruhr-University Bochum, 44892 Bochum, Germany.

2 Department of Neurosurgery, University Hospital Erlangen, 91054 Erlangen, Germany.

3 Department of Neurosurgery, University Hospital Halle (Saale), 06120 Halle, Germany.

4 Department of Neurosurgery, University Hospital Knappschaftskrankenhaus, Ruhr-University, 44892 Bochum, Germany.

5 Besa, GmbH, 82166 Gräfeling, Germany.

6 Institute for Biomagnetism und Biosignalanalysis, University of Münster, 48149 Münster, Germany.

7 Otto Creutzfeldt Center for Cognitive and Behavioral Neuroscience, University of Münster, 48149 Münster, Germany.

Correspondence to: Kanjana Unnwongse, MD
Ruhr Epileptologie, Neurologische Klinik,
Universitätsklinikum Knappschaftskrankenhaus Bochum
In der Schornau 23-25
44892 Bochum, Germany
Email: kanjana.unnwongse@kk-bochum.de

Abstract

Electrical source imaging is used in the presurgical epilepsy evaluation and in cognitive neurosciences to localize neuronal sources of brain potentials recorded on EEG. This study evaluates spatial accuracy of electrical source imaging for known sources, using electrical stimulation potentials recorded on simultaneous stereo-EEG and 37-electrode scalp EEG, and identifies factors determining the localization error.

In 11 patients undergoing simultaneous stereo-EEG and 37-electrode scalp EEG recordings, sequential series of 99-110 biphasic pulses (2-millisecond pulse width) were applied by bipolar electrical stimulation on adjacent contacts of implanted stereo-EEG electrodes. The scalp EEG correlates of stimulation potentials were recorded with a sampling rate of 30 kHz. Electrical source imaging of averaged stimulation potentials was calculated utilizing a dipole source model of peak stimulation potentials based on individual four compartment finite element method head models with various skull conductivities (range from 0.0413 to 0.001 S/m). Fitted dipoles with goodness of fit of ≥80% were included into the analysis. The localization error was calculated using Euclidean distance between the estimated dipoles and the center point of adjacent stimulating contacts.

A total of 3,619 stimulation locations, respectively dipole localizations, were included in the evaluation. Mean localization errors ranged from 10.3 to 26 mm, depending on source depth and selected skull conductivity. The mean localization error increased with an increase of source depth (r (3,617) = [0.19], P = 0.000) and decreased with an increase of skull conductivity (r (3,617) = [-0.26], P = 0.000). High skull conductivities (0.0413-0.0118 S/m) yielded significantly lower localization errors for all source depths. For superficial sources (<20 mm from inner skull), all skull conductivities yielded insignificantly different localization error. However, for deeper sources, in particular > 40 mm, high skull conductivities of 0.0413 and 0.0206 S/m yielded significantly lower localization errors. In relation to stimulation locations, the majority of estimated dipoles moved outward-forward-downward to inward-forward-downward with a decrease of source depth and an increase of skull conductivity. Multivariate analysis revealed that an increase of source depth, number of skull holes, and white matter volume, while decrease of skull conductivity independently led to higher localization error.

This evaluation of electrical source imaging accuracy using artificial patterns with high signal to noise ratio supports its application in presurgical epilepsy evaluation and cognitive

neurosciences. In our artificial potentials model, optimizing the selected skull conductivity minimized the localization error. Future studies should examine if this accounts for true neural signals.

Running title: Validating EEG source imaging

Keywords: source analysis; source reconstruction; source localization; inverse solution; head volume conductor modeling

Abbreviations: β = unstandardized coefficient; BEM = boundary element method; DAC = directly applied current; dSPM = dynamic Statistical Parametric Maps; EIT = electrical impedance tomography; eLORETA = exact Low Resolution Electromagnetic Tomography; E/MEG = electromagnetic data; ESI = electrical source imaging; FEM = finite element method; fMRI = functional MRI; GoF = goodness of fit; HFOs = high frequency oscillations; IFCN = International Federation of Clinical Neurophysiology; MNE = Minimum Norm Estimate; MPRAGE = Magnetization Prepared Rapid Gradient Echo Imaging; *r* = correlation coefficient; SD = standard deviation; SSCR = skull: scalp conductivity ratio; SPECT = single-photon emission computerized tomography

Introduction

Electrical source imaging (ESI) of interictal and ictal epileptic activity has become an applied diagnostic tool in the presurgical epilepsy evaluation.[1-5] In epilepsy cases with concordant findings, ESI strengthens a hypothesis on the localization of the epileptogenic zone (focus hypothesis) which is based on seizure semiology, visual evaluation of interictal and ictal EEG, and MRI with epilepsy-specific sequences. In cases with discordant findings, possibly multifocal or non-lesional pharmaco-resistant epilepsies, ESI is applied to narrow the focus hypothesis.[6-8] In particular, in non-lesional epilepsy, the result of interictal ESI serves to define targets of intracranial EEG electrode placement when the ictal onset on scalp EEG is not localizable or when the ictal onset is in the vicinity of eloquent cortex.[9-11] Technically comparable, the analysis of event related potentials on EEG intends to localize

neurophysiological processes in the brain.[12-13] In either scenario, high spatial accuracy is essential. An ESI error of 2-3 cm might not affect decisions with regard to lobar resection, but is relevant for small resections, placement of intracranial electrodes or trajectories for radiofrequency or laser thermocoagulation.

A range of factors has been shown to influence spatial accuracy of ESI. One of the most relevant is the number and coverage of EEG electrodes.[1,11,14] Especially the use of additional infratemporal electrodes has demonstrated a positive effect on accuracy.[15] The IFCN has recently published recommendations on a standard array including six electrodes of the inferior temporal chain, to capture epileptic activity from mesial temporal structures[16,17]. However, numerous further important aspects of ESI have considerable impact, including applied head models,[18-21] selected tissue conductivities,[20,21] different inverse methods,[5,24] spike selection and clustering,[25] and time-point of ESI related to the spike (peak, half rising or spike onset).[26,27] In particular choosing optimal skull conductivity might be the most challenging, given that skull conductivity values are known to vary inter- and intra-individually and depending on measurement methods (in vivo, ex vivo or in vitro)[28,29]. Most available studies focus on diagnostic accuracy and clinical utility of ESI based on external validation. Namely, the concordance of ESI results with resection volume is evaluated in relation to postoperative seizure control.[9,10,30] Since resection volumes may measure several centimeters in diameter, such studies, while clinically relevant, yield only coarse and indirect information on spatial accuracy of ESI. Correspondingly, comparison of ESI results with surgical resection volumes tends to overestimate specificity. Similarly, other studies report the overlap of ESI results with the focus hypothesis derived from other presurgical investigation techniques such as MRI (lesional and non-lesional), PET, single-photon emission computerized tomography (SPECT), magnetic source imaging, EEG-fMRI or electrocorticography, which also provide limited data on spatial accuracy.[2,10,31-34]

Results of studies validating ESI with consecutive intracranial EEG recordings may however suffer from limitations due to the variability of epileptic activity.[12,26,35,36] It ultimately remains unclear whether ESI was calculated on patterns that are truly comparable to findings in the intracranial EEG, which may have been recorded weeks or months after the scalp EEG recordings. Ideally, ESI spatial accuracy should be evaluated using the same signal recorded simultaneously with both scalp and intracranial EEG.[37,38] Probably due to the logistic effort required to combine scalp and intracranial EEG recordings, such studies are sparse. Comparison of ESI with stereo-EEG using such recordings found that the equivalent current

dipole localization was on average 47.2 ± 23.2 mm away from the stereo-EEG seizure onset[39]. While in another study using dipole and maximum distributed source, the median distance error to the centroid of seizure onset electrodes was 30-33 mm[40]. However, validation of these studies is limited by subjective EEG seizure interpretation and restricted spatial sampling of stereo-EEG electrodes[41].

The presented study therefore aims to evaluate the spatial accuracy of ESI using simultaneous stereo-EEG and 37-electrode scalp EEG during intracranial presurgical evaluation. To establish ground-truth localizations, we employed bipolar electrical stimulation of adjacent stereo-EEG contacts. ESI of the scalp EEG correlate of the stimulation potential was analyzed and localization errors were calculated.

Materials and methods

Eleven patients who underwent intracranial stereo-EEG recordings as part of their presurgical evaluation for pharmaco-resistant focal epilepsy were studied. The decision to implant patients was made by a multidisciplinary team based on clinical parameters without consideration of the presented study. This study (register number: 20-6970) was approved by the ethics commission of the faculty of medicine, Ruhr-Universität Bochum, Germany. Simultaneous intracranial stereo-EEG and 37-electrode scalp EEG (10-20 system with additional paracentral and inferior frontal-temporal electrodes, Supplementary Fig. 1) was recorded for 1-3 weeks until a sufficient amount of interictal and ictal data was recorded. Number and placement of intracranial electrodes were determined according to the clinical context and the results of previous non-invasive evaluation and were not influenced by the goals of the presented study. Electrical stimulation was a part of our clinical evaluation during intracranial EEG recording.[42] Stereo-EEG electrodes (AD-tech, Racine, WI, USA) with diameter of 1.1 mm, contact length of 2.4 mm, and inter-spacing length of 2.1 mm were used. Intracranial single-pulse electrostimulation (ISIS Stimulator, Inomed Medizintechnik GmbH, Emmendigen, Germany) of biphasic pulses (2-millisecond pulse width) at 1 Hz, 1 mA intensity, 99-110 trials, were applied on adjacent contact pairs in bipolar fashion. Stimulation potentials on simultaneous stereo-EEG and 37-electrode scalp EEG were recorded on NeuroPort™ (Blackrock Microsystems, UT, USA) with a sampling rate of 30,000 Hz. Steps of the workflow are shown in Fig. 1.

Electrode localization

Isotropic T1 3D-MPRAGE volume MRI was acquired using a 3T scanner (MAGNETOM Prisma 3.0T, Erlangen, Germany) before implantation of intracranial electrodes. Post-implantation CT (CT Elekta 1.0, Stockholm, Sweden) was acquired for localizing stereo-EEG and scalp EEG electrodes within 24 hours after implantation. Electrodes were segmented using the post-implantation CT-dataset. Individual stereo-EEG and scalp EEG contacts were labeled manually according to the clinical documentation. The CT dataset was then co-registered to pre-implantation MRI using a mutual information approach (Curry 7, Compumedics Neuroscan, USA, Fig. 1C)[43]. The resulting co-registered scalp electrode positions were used for ESI. The pre-operative MRI was registered in Talairach space, which subsequently allowed expressing electrode localizations from CT in standardized Talairach co-ordinates and grouping according to anatomical regions. This whole process of electrode localization was done by one author (SR) in all patients. The locations of electrode contacts in different brain tissues (i.e., deep grey matter, white matter, grey-white matter junction and superficial grey matter) were visually identified by one author (KU) using post-implantation MRI.

Electrical source imaging

Stimulation potentials were detected using a template search algorithm (BESA Research 6.1, BESA GmbH, Gräfeling, Germany). Templates, channels and settings for the automated search were selected manually. Detection results were checked for correctness and excessive additional artifacts. Scalp channels and few trials with excessive noise, flat lines, etc. based on visual inspection were rejected (Fig. 1A). Stimulation potentials (99-110 trials) with an epoch length of -250 to 150 milliseconds were then averaged. All filters (low and high pass as well as notch filters) were turned off, regularization was set to zero, and baseline fit was set to -250 to -50 milliseconds avoiding overlap with the stimulation pattern. A regional dipole was fitted from the onset to the negative peak with a fit interval of -1.5 to 0 milliseconds of each averaged stimulation potential (Fig. 1D). ESI was done by one author, KU. Fitted dipoles with goodness of fit (GoF) of ≥ 80% were included in the analysis. An individual four compartment finite element method (FEM) model with separate conductivity values of scalp (0.33 S/m), CSF (1.79 S/m), brain (0.33 S/m) and various skull conductivities was used (BESA MRI 2.0, BESA GmbH, Gräfeling, Germany). Values for skull conductivity were 0.0413, 0.0206, 0.0138, 0.0118, 0.01, 0.008, 0.006, 0.0047, 0.0042, 0.002 and 0.001

S/m, corresponding to a skull: scalp conductivity ratio (SSCR) of 1: 8, 16, 24, 28, 33, 41, 55, 70, 80, 165 and 330 respectively (Fig. 1B). We used SSCR instead of BSCR (brain: skull conductivity ratio) because brain compartment has the same conductivity value as scalp compartment and scalp and skull conductivity values are the most sensitive parameters on the EEG measurement.[21] Each stimulation run (99-10 trials) using adjacent stereo-EEG contact pair thus yielded one averaged stimulation potential and subsequently one estimated dipole for each selected skull conductivity value. The coordinates of the estimated dipole and the center point between adjacent stimulating contact pair expressed as Talairach co-ordinates were determined. The Euclidean distance between these coordinates defined the localization error (Fig. 1E). Source depth was measured by the shortest distance from the inner skull (hull) to the center of stimulating contact pair. The offset direction was determined by the deviation of the estimated dipole from the center of the stimulating contact pair along the horizontal, anterior-posterior and vertical axes of the head.

Statistical analysis

Due to normally distributed data, mean and standard deviation were reported to present the center and dispersion of the data. Relationship between the localization error and source depths as well as relationship between the localization error and skull conductivities were determined using curve estimation on SPSS 16.0 (IBM, New York, USA) to find a best-fit model. Pearson correlation was used to measure the strength of correlation between variables. One-way analysis of variance (ANOVA) and post-hoc (Bonferroni) test were performed to compare the effect of selected skull conductivity values on mean localization errors at different source depths. Independent predicting factors of localization errors were identified using multiple linear regression (forward method).

Data availability

The data that support the findings of this study are available from the corresponding author, upon reasonable request.

Results

Eleven patients with pharmaco-resistant focal epilepsy undergoing intracranial evaluation with stereo-EEG electrodes implantation during 2016-2018 were enrolled. A mean of six stereo-EEG electrodes (range 2-11) was implanted per patient with a mean of nine contacts (range 4-14) per electrode. In total, there were 620 contacts of 67 stereo-EEG electrodes. Fifty-five stereo-EEG electrodes were implanted in temporal lobes and the remainder were located in frontal lobes (Supplementary Fig. 2). Stimulation was applied across 553 contact pairs. EEG data from 212 contact pairs were excluded due to abundant artifacts (n=108), amplitudes exceeding the amplifier's dynamic range (n=72) or incomplete stimulation trials (n=32). Using the remaining contact pairs, 341 averaged stimulation potentials from nine patients (two women) were analyzed with ESI, using 11 different skull conductivity values, resulting in 3,751 estimated dipoles. Finally, 3,619 (96.5%) fitted dipoles with goodness of fit ≥80% were included into the analysis of localization errors (Fig. 2).

One hundred thirty-two (3.5%) fitted dipoles showed a goodness of fit <80%. These fitted dipoles were derived, using 11 skull conductivity values, from ESI of 15 averaged stimulation potentials generated in 4 electrodes. Three of those electrodes belonged to one patient. One hundred and ten (83%) of these fitted dipoles had an average GoF of 75% (range 63-79), while the rest had an average GoF of 54% (range 50-60). Possible explanations of this low GoF are (i) technical issues such as contaminated data during stimulation or a defect of the particular electrodes as well as (ii) distribution of scalp EEG electrodes of this particular patient did not cover both poles of the dipolar potential topography well enough.

Localization error of estimated dipoles

Plots of mean localization errors against source depths across various skull conductivity values showed linear relationships based on curve fit analysis (R^2 = 0.04, F (1, 3,617) = 136.8, P = 0.000). Overall, higher mean localization errors were observed with deeper source depth (r (3,617) = [0.19], P = 0.000, Fig. 3). Moderate correlations of these two variables were found when using SSCR 1:165 and 1:330 (r (325) = [0.49], P = 0.000 and r (324) = [0.55], P = 0.000), and weak correlations were found when using SSCR 1:41 to 1:80 (r (325-332) = [0.26-0.38], P = 0.000). Using even higher skull conductivities (SSCR 1:8 and 1:16), the correlation of these two variables became inverse (r (333) = [-0.42], P = 0.000 and r (328) = [-0.18], P = 0.001), that is higher mean localization errors were observed with more superficial source depth.

Plots of mean localization errors against skull conductivities across various depths mainly showed inverse linear relationships (R^2 = 0.07, F (1, 3,617) = 251.1, P = 0.000), that is higher mean localization errors were observed when using lower skull conductivity (r (3,617) = [-0.26], P = 0.000, Fig. 4). Moderate correlations of these two variables were found at source depths of >30-40 mm and >40 mm (r (1,002) = [-0.53], P = 0.000 and r (446) = [-0.58], P = 0.000), and weak correlations were found at source depths of >20-30 mm (r (1,095) = [-0.2], P = 0.000). At more superficial source depths (≤20 mm), correlations were reverse to linear, that is higher mean localization errors were associated with higher skull conductivities; however, these correlations were not statistically significant.

Using the standard adult skull conductivity (SSCR 1:80), mean localization errors ranged from 14.4 mm at source depth of ≤10 mm to 23.4 mm at source depth of >40 mm with *SD* of 7 and 6.4 mm respectively (Table 1). At source depth ≤20 mm, one-way ANOVA revealed no significant differences in mean localization errors when using different skull conductivities from SSCR of 1:8 to 1:330. At source depth of >20 mm, one-way ANOVA revealed significantly lower mean localization errors when using higher skull conductivity values (>20-30 mm: F (10, 1,086) = 13.93, P <0.01, >30-40 mm: F (10, 993) = 71.48, P <0.01, >40 mm: F (10, 437) = 32.65, P <0.01). Multiple comparisons (Bonferroni test) revealed that at source depth of >40 mm, SSCR of 1:8 yielded the lowest mean localization error, however not significantly different from the error provided by SSCR of 1:16 (P = 1.0). At source depth of >30-40 mm, SSCR of 1:8 yielded the lowest mean localization error, not significantly different to from the errors provided by SSCR of 1:16 and 1:24 (P = 1.0). At source depth of >20-30 mm, SSCR of 1:16 yielded the lowest mean localization error, not significantly different to from the errors provided by SSCR of 1:8 and 1:24 to 1:55 (P = 1.0). Across all depth ranges, the skull conductivities that yielded the lowest mean localization errors was SSCR of 1:16, however not significantly different from the errors provided by SSCR of 1:8, 1:24 and 1:28 (one-way ANOVA: F (10, 3068) = 50.89, P <0.01 & Bonferroni test P = 1.0). Using the standard adult skull conductivity, mean localization errors of 22.1 (*SD*±7), 18.1 (±6.5), 17.7 (±6.1) and 15.6 (±7.3) mm were observed with sources located in deep grey, white, grey-white and superficial grey tissues, respectively. The mean localization error with sources located in mesial temporal structures (including hippocampus, amygdala, parahippocampal gyrus and fusiform gyrus), lateral temporal cortex, lateral frontal cortex and mesial frontal cortex were 22.5 (*SD*±6.1), 14.4 (±5), 15.4 (±8.6) and 34.7 (±4.5) mm, respectively.

Offset direction of estimated dipoles

The offset direction of estimated dipoles in relation to stimulation locations were evaluated in regards to the hemisphere, along the three axes of the Talairach coordinate system: horizontal in-out (X-axis), anterior-posterior (Y-axis) and vertical (Z-axis). On the horizontal axis, using a skull conductivity of 0.008 S/m (SSCR 1:41) and lower, 79%, 90%, 78%, 51% and 29% of estimated dipoles, observed at source depths >40 mm, >30-40 mm, >20-30 mm, >10-20 mm and ≤10 mm respectively, moved outward from the center of the head (Fig. 5). On the contrary, using SSCR higher than 1:41, 56%, 43%, 62%, 77% and 89% of estimated dipoles, observed at source depths >40 mm, >30-40 mm, >20-30 mm, >10-20 mm and ≤10 mm, respectively, moved inward to the center of the head. On the anterior-posterior axis, the majority of estimated dipoles (80%) across various source depths and skull conductivities moved forward to the front of the head. Only few estimated dipoles from source depths of ≤30 mm using high skull conductivities (SSCR 1:8 and 1:16) moved backward. On the vertical axis, across various skull conductivities, the majority of estimated dipoles (80%) observed at source depths >40 mm, >30-40 mm and ≤10 mm moved downward towards the skull base. About 50% of estimated dipoles observed at remaining source depths moved downward. Overall, the offset direction mainly changed from outward-forward-downward to inward-forward-downward with a decrease of source depth and an increase of skull conductivity.

Using the standard adult skull conductivity (SSCR 1:80), the offset direction of estimated dipoles with sources located in mesial temporal structures (depth >40 mm) mainly shifted outward-forward-downward (67%) (Fig. 6). The offset direction of estimated dipoles with sources located in lateral temporal cortex (depth >10-30 mm) shifted outward-forward-downward for 26%, outward-forward-upward for 22% and inward-forward-downward as well as inward-forward-upward for 18%. The offset direction of estimated dipoles with sources located in lateral frontal cortex (depth ≤10 mm) shifted inward-forward-downward for 31% and outward-forward-downward for 21%.

Further factors determining localization error

In multiple linear regression, the overall regression was statistically significant (R^2 = 0.25, F (1, 3,609) = 23.4, P = 0.000), and four variables independently determining localization error were identified. Increase of source depth (β = 0.11; *95%CI*, [0.09, 1.13]), number of skull

burr holes related to the implantation of SEEG electrodes (β = 0.89; *95%CI* [0.79, 0.99]) and white matter volume (β = 0.04; *95%CI* [0.03, 0.05]) as well as decreased skull conductivity (β = -154.4; *95%CI* [-137.3, -171.5]) were associated with increased localization errors. This means that a 1 mm increment of source depth resulted in a localization error increase of 0.11 mm and with every 0.01 S/m decrement of skull conductivity, the localization error increased by 1.5 mm. One additional burr hole and 1 mm^3 increment of white matter volume would increase localization error by 0.9 and 0.04 mm respectively. Of the categorical variables, gender and anatomical region differences influenced localization errors. The two women had higher localization errors than men (β = 2.2; *95%CI* [1.63, 2.76]). In comparison to sources located in the mesial temporal structures, sources located in the mesial frontal region had higher localization errors (β = 13.5; *95%CI* [11.5, 15.5]) while sources located in the lateral temporal cortex (β = -1.49; *95%CI* [-2.1, -0.89] had lower localization errors. Grey matter and CSF volumes, skull thickness, number of stereo-EEG contacts, and the subject's age and whether stimulating contacts were located in grey or white matter did not show a systematic association with the localization error.

Discussion

The present study evaluated the accuracy of ESI by measuring the localization error between the estimated dipole, analyzed from the averaged stimulation potential, recorded on 37-electrode scalp EEG, and its known source, that is the center point between stimulating stereo-EEG contact pair. The main findings are that the mean localization error increased with an increase of source depth and a decrease of skull conductivity. Using standard adult skull conductivity (SSCR 1:80), the mean localization error of source depths 0.4-47.8 mm was 14.4-23.4 mm. Skull conductivity values of 0.0413-0.0118 S/m or SSCR 1:8 to 1:28 yielded the significantly lower localization errors across all source depths. In relation to stimulation locations, the majority of estimated dipoles moved outward-forward-downward to inward-forward-downward with a decrease of source depth and an increase of skull conductivity.

Localization error of estimated dipoles in relation to source depth and skull conductivity

The localization error associated with the source depth has been tested previously using electrical stimulation potentials or dipole simulation as the ground truth. In comparison to our study, these studies evaluated smaller number of stimulation locations or simulated dipoles, a limited number of scalp EEG electrodes (21 electrodes, 10-20 EEG system), a spherical or boundary element method (BEM) head model, one selected skull conductivity value and different inverse solutions during ESI (Table 2). Cuffin *et al*.[44] reported an average localization error of 11 mm (maximum 25.7 mm) based on analysis of 28 stimulation potentials with an unclear relationship between the localization error and the source depth. Krings *et al*.[45] using 21 EEG electrodes found that the average localization errors of stimulating contacts located shallower in the temporal lobe (40-57 mm depth) were higher than errors of deeper contacts (62-85 mm depth). However, when adding 20 more electrodes on the anterior half of the head, according to the 10-10 EEG system, the average localization errors of deeper contacts were higher. The depth of sources in Krings *et al*.[45] study was much deeper than in our study. However their average localization error observed using 41 scalp electrodes at source depth 40-57 mm, was comparable to our average localization error at source depth >40 mm (19.3 vs 23.4±6.4 mm, Table 1). In line with our findings, a dipole simulation study by Roth *et al*.[46] showed that dipoles located in the mesial temporal area had higher localization errors than those located in the lateral and anterior temporal lobe or insula, with an average localization error of 19.7 mm (maximum 42 mm). Within the source depth range of 6-69 mm, Yvert *et al*.[47] reported that the average localization error decreased with increasing source depth, discordant to our findings (Fig. 3). This probably resulted from numerical forward errors due to suboptimal mesh resolution. Our study used an appropriate mesh resolution thus numerical errors are assumedly negligible. With a higher number of simulated dipoles (n = 92), Whittingstall *et al*.[48], 2003 found that the average localization error increased with an increase of source depth, similar to our findings, but ranges of error were rather wide (~30 mm). By means of electrical stimulation (61 locations), 256-electrode scalp EEG recording and realistically BEM as volume conductor model, Mikulan *et al*.[49] showed that the choice of inverse solution method employed during ESI affects the relationship between localization error and source depth. Using Minimum Norm Estimate (MNE) and exact Low Resolution Electromagnetic Tomography (eLORETA), the

localization error increased with an increase of source depth with a strong correlation found for MNE (β = 0.7, r^2 = 0.71). While using dynamic Statistical Parametric Maps (dSPM), the localization error increased with a decrease of source depth, with a weak correlation (β = -0.27, r^2 = 0.27). Of note, inverse solution is referred to a calculation of source characteristics from the measured (brain) potential distributions by considering the evolution of topographies over time (ESI), whereas forward solution is referred to a calculation of a (brain) potential and its topography from a source with known characteristics.

In summary, the relationship between the localization error and the source depth observed from previous studies is likely influenced by factors including inverse solution methods, number of scalp EEG electrodes, depth of ground truth (source), number of measured stimulation locations or simulated dipoles, and accuracy of head modeling. Due to the simple and well-controlled source model as well as the well-validated dipole fit approach in our study, we are confident that the part of the error due to the inverse modeling is rather negligible. Errors are rather due to limited sensor number and coverage as well as limited forward modeling accuracy. To the best of our knowledge, this present study is the first to evaluate large number of stimulation potentials of known dipolar sources (n = 3,619) recorded simultaneously on stereo-EEG and scalp EEG, using dipole fit approaches in realistically-shaped four compartment FEM models: We found that an increase of source depth independently led to higher localization error.

Selection of skull conductivities plays an important part in solving the forward and inverse problem in ESI and significantly influences the localization accuracy in relation to source depth.[23,50-52] Wang *et al.*[53] found that if skull conductivities (SSCR 1:15 to 1:25) used for inverse solutions were higher than the conductivity (SSCR 1:80) used for the forward solution during the simulation, the localization error of deep sources (i.e., hippocampus) became lower. Conversely, if the skull conductivity used for the inverse solution was lower than the one used for the forward calculation, the localization error of superficial sources became lower. This is concordant to our finding that using an exceedingly high skull conductivity would result in a relatively low localization error for deep sources and a relatively high error for superficial sources (Fig. 4). Such over-estimation of skull conductivity moves the estimated dipole deeper into the brain.[54,55] It is important to note that there is a methodological limit to this error, since the maximum depth in the source space is the center of the head. This means that superficial sources have a larger "potential error range" compared to deep sources. On the other hand, under-estimation of skull conductivity

moves the estimated dipole closer to the inner skull. This effect is limited by the superficial boundary of the source space. Thus deep sources, which have a larger potential error range, result in higher dipole localization errors. Currently, determination of individual skull conductivity is not feasible in a clinical setting. Based on a series of in vivo measurements, a SSCR of 1:15 may be more adequate than the standard SSCR of 1:80 due to its yield of higher accuracy.[56] Conductivity values of the homogenized skull compartment are known to vary due to inter- and intra-subject variability and different measurement methods (in vivo, ex vivo or in vitro). In a meta-analysis of 20 studies, whole skull conductivity varied significantly, depending on the employed methodology (P= 0.02). Values for the whole skull conductivity obtained from electrical impedance tomography (EIT ~0.006 S/m) were significantly lower than those obtained from directly applied current (DAC ~0.0125 S/m) and electromagnetic data (E/MEG ~0.013 S/m). Based on 99 conductivity values from 121 participants in these 20 studies, a weighted average mean skull conductivity, calculated by taking into consideration the quality of each study was 0.016 ± 0.019 S/m[28]. This recommended value overlaps our range of skull conductivities (0.0413-0.0118 S/m; SSCR 1:8 to1:28) that yielded the significantly lower localization errors for all source depths. In particular, for sources deeper than 40 mm from the inner skull, SSCR 1:8 (0.0413 S/m) and 1:16 (0.0206 S/m) provided significantly lower localization errors compared to other conductivity values. However, due to inter-subject variability of skull conductivity and thickness, this common value may still result in considerable inaccuracies.[29] If subject-specific calibrated realistic head models are not available, using a Bayesian uncertainty model with regard to unknown skull conductivity may result in improved localization.[29,55]

Evaluation of a broad range of skull conductivities in this study was influenced by our previous work[50]. Following our experience on the difficulty of inter- and intra-subject variability in head tissue conductivities, using a scalp conductivity lower than 8 times skull conductivity (SSCR <1:8) is unrealistic for adult patients. Due to a gap in the range of evaluated SSCR between 1:16 and 1:8, we do not know if the localization error function is rather L-shaped or U-shaped. In case of a U-shaped function, the minimum might be between the 1:16 and 1:8 ratios, while an L-shaped curve might be explained by constant localization errors as a result of using high skull conductivities for deep sources (Fig. 4). For deep sources (>40 mm), changes in skull conductivity influenced source magnitude rather than source localization.

Offset direction of estimated dipoles

Previous studies reported the largest localization errors on the vertical axis with a marked downward shift of estimated dipoles.[45,46] This may be caused by the limited electrode coverage of the inferior head by the 10-20 scalp EEG system. A whole head coverage, including face and neck, reduced the localization error for anterior temporal spikes because inferior head channels were important in measuring the ventral field distribution of the spikes.[15] A hypothetical "full cap" with evenly spaced electrodes around the entire head including the area below the skull base reduced localization errors in the centimeter range, compared to a realistic high-density EEG cap.[57] Our mean localization error was smallest 7.6 (*SD*±6.1) on the vertical axis, followed by 7.8 (±5.1) mm error on the anterior-posterior axis and 8.2 (±6.5) mm error on the horizontal axis. The additional inferior frontal-temporal coverage in our 37-electrode scalp EEG likely reduced the localization error on the vertical axis. A forward shift of estimated dipoles was observed using the 10-20 EEG system, but with an additional electrodes according to 10-10 EEG system on the anterior aspect of the head, resulted in an opposite direction shift towards the back of the head, where number of electrodes was lower.[45] However our 37-electrode, 10-20 EEG system with additional paracentral and inferior fronto-temporal coverage, we again observed shifts in forward direction of estimated dipoles. Our offset direction on the horizontal axis was mainly influenced by the selected skull conductivity applied during ESI.

Further factors determining the localization error

We also found in multivariate analysis that the localization error increased with increasing white matter volume, however the effect size was small compared to the other factors discussed above. To the best of our knowledge, no studies have reported on the relationship between brain tissue volume and localization error. However, available evidence regarding the effects of tissue resistivity and anisotropy can at least in part explain our finding. Electric surface potentials (EEG) are sensitive to changes in resistivity of the tissues located between the source and the scalp electrode.[58-60] Tissue resistivity influenced ESI localization to a similar degree as anisotropy of gray and white matter.[61] Sources placed in the sulcus next to white matter shifted >5 mm farther outwards and even more so when the source was surrounded by large white matter tracts, in particular if anisotropic conductivity of white

matter tissue was neglected in the FEM model.[62-64] Inclusion of the gray/white matter distinction affected EEG magnitude and topography, which had implications for ESI localization.[19,21,65,66] While using a realistically shaped four compartment (scalp, skull, brain and CSF) FEM approach based on individual MRI, our head model still has limitations. Our individual FEM did not include scalp, grey and white matter conductivities that vary from one to another.[23,67] Neither did we model other tissues such as dura and blood vessels.[68-69] It is conceivable that inclusion of these tissue types could create more accurate volume conduction models. Scalp conductivity uncertainties significantly influence on EEG source localization, however in a lesser degree, compare to skull conductivity.[23] Conductivity uncertainties of grey matter rather influence on EEG forward solution than source localization, while white matter mainly affect orientation of reconstructed sources.[23] Further studies are required to clarify how the volume conduction parameters discussed above relate to ESI localization error.

Studies investigating the effect of skull defects on the localization error found errors of up to 10 mm when not modelling skull holes with a diameter of 5-20 mm in a volume conductor model using three compartment (scalp, skull and brain) FEM models.[50,70,71] Using five compartment (scalp, compact bone, cancellous bone, brain and CSF)) FEM models, if a skull hole was >6 mm in diameter and located in the proximity of the source, mean localization errors of only 1 mm were observed. A 2 mm diameter skull hole as used in our study resulted in negligible errors.[71] However, we found that the localization error increased with the number of these ~2 mm holes related to stereo-EEG electrode implantation, the estimated impact was approximately 0.9 mm per hole.

Influence of sex on localization accuracy was observed in our study. Women show a significant decrease of skull thickness (30-60%) with increasing age.[72] Both an increase of age and a decrease of skull thickness are associated with a decrease of the skull conductivity.[29,73] The thickness of scalp layers varies with age and sex owing to hormonal differences.[74] Local variations in skull and scalp thickness affect localization errors of about 1-6 mm.[71,75,76] Based on these findings, it is conceivable that higher localization errors in women in our study may be due to differences in skull and scalp thickness. However, due to the low sample size of our cohort, a robust comparison was not possible.

Lastly, we found that sources located in mesial temporal and frontal areas and had higher localization errors than sources located in lateral temporal and frontal cortices. Potentially

due to the more sophisticated volume conductor model and the discrepancy of the anisotropic ratio in the mesial areas near the gray-white matter boundary together with a limited electrode coverage, large localization errors were reported for sources located mainly in the mesial and the basal aspects of the brain.[63] Significant EEG magnitude and topography changes were found near interhemispheric and Sylvian fissures if the larger CSF spaces in these areas were included in the head models.[19,21,77] Moreover, sources in the basal aspect were susceptible to localization errors due to skull geometry, i.e. sinuses and thickness of the skull base if those were not modeled.[71]

Limitations and future directions

We acknowledge the following limitations. First, our ESI results were based on 37 EEG electrodes placed according to the 10-20 system with additional paracentral and inferior frontal-temporal coverage. This comparably low number of electrodes may have diminished the accuracy of ESI in the range of few millimeters to centimeters.[50,78,79] In terms of diagnostic accuracy, a recent meta-analysis of both interictal and ictal source imaging for successful epilepsy surgery reported no significant differences of sensitivity, specificity and accuracy of ESI obtained from low (19-32) and high (65-256 electrodes) density EEG recordings.[3] Simulation studies investigating spatial accuracy of ESI showed significant influence of both the number of electrodes and their extended inferior coverage on the localization error.[15,57] Due to intrinsic limitations of volume conductor models and inverse solutions, localization errors were observed even when a high number of scalp electrodes were used in simulation studies and studies using electrical stimulation as known sources.[49,79] In our experience, 37electrodes scalp video-EEG monitoring for presurgical evaluation is feasible over several days, tolerable for patients and has limited additional technical requirements, while increasing the yield for epileptic activity. With 37 electrodes EEG, our mean localization error of ESI using standard adult skull conductivity was 14.4-23.4 mm from source depth of 0.4-47.8 mm. This error compares favorably to the evaluation of lesions[79], resection[1,9,81] and intracranial EEG.[30,82] Nevertheless, further reducing this error must be the goal of future research. A further limitation is that the true skull conductivity values of individual patients were not available. Instead, we explored a range of skull conductivity values concerning the impact on ESI localization errors. Moreover, we did not vary tissue conductivity and include anisotropy of various compartments that influence

localization accuracy in our head models, due to methodological and logistical limitations of our analysis pipeline and the applied software.[62,63,67,68,70,83,84] The effect of exclusion of the stereo-EEG from our head models however might be negligible since our electric sources were Venant dipole sources around stereo-EEG contacts.[23,85,86] Another limitation is that the stimulation potentials we examined probably have a much higher signal-to-noise ratio and not necessarily exactly reflect the signal characteristics of true epileptic activity. Due to the attenuating property of the skull, the generating source of interictal epileptic activity is estimated to be at least 6-10 cm^2 in order to be recognized on scalp EEG.[37,38] For high frequency oscillations (HFOs), one or few small asynchronous oscillatory sources of about 1 cm^2 contribute to scalp EEG[87]. However, the signal-to-noise ratio of less than one in this case would make it difficult or even impossible to robustly detect such patterns. Thus the accuracy of ESI of patterns with lower signal-to-noise ratios and less focal generators, such as HFOs and interictal epileptic activities, is likely to be lower, compared to the artificial stimulation potentials used in our study. Our findings might thus overestimate the accuracy of ESI, or at least represent a best-case scenario.

Moreover, there were intrinsic constraints of ESI that contribute to our remaining localization error. For once it is based on the quasi-static approach to Maxwell's equations, ignoring capacitive, inductive as well as propagation effects might contribute to our remaining localization error.[88,89] Lastly, the finite element method, implemented in BESA MRI, uses the Saint Venant source modeling approach. This method models a mathematical dipole source by means of a small cloud of monopolar sources in the close neighborhood, which best approximate the intended dipolar moment. It assumes that the source is located in grey matter.[90] In our study, this assumption holds when the two stimulating contacts are both in grey matter, however, if the stimulating contacts are in different tissues with different conductivities, the quality of the source model might suffer. In the future, a sensitivity study should be carried out to simulate these effects using for example a two-monopolar source.

Our findings of area-specific localization error magnitude and offset direction may be used to implement an error map that would allow annotating ESI results with information regarding the likely magnitude and direction of its mis-localization. Furthermore, individual skull conductivity could be calibrated using ESI of simultaneous intracranial and scalp EEG that would enable optimization of ESI results from previous scalp EEG recordings. Although such optimization would be late during presurgical evaluation, the findings might be informative for further electrode implantation or resection planning. However, such applications would

have to be validated prospectively in a larger patient population considering different brain locations, higher number of scalp EEG electrodes, more detailed head volume conductor models, etc.

Funding

This study was performed without extramural funding. The Förderverein Ruhr-Epileptology (friends and supporters of Ruhr-Epileptology) covered administrative expenses for the study such as ethics committee fees.

CHW and SR are supported by Deutsche Forschungsgemeinschaft, projects WO1425/10-1 and RA 2062/1-1, and the Bundesministerium für Gesundheit project ZMI1-2521FSB006, under the frame of European Research Area Personalized Medicine project ERAPERMED2020-227 to CHW.

Competing interests

MR is an employee of BESA GmbH, a company, which develops and provides software tools for EEG and MEG data analysis.

References

1. Brodbeck V, Spinelli L, Lascano A et al. Electroencephalographic source imaging: a prospective study of 152 operated epileptic patients. *Brain*. 2011;134(10):2887-2897.
2. Sharma P, Scherg M, Pinborg L et al. Ictal and interictal electric source imaging in pre-surgical evaluation: a prospective study. *Eur J Neurol*. 2018;25(9):1154-1160.
3. Sharma P, Seeck M, Beniczky S. Accuracy of Interictal and Ictal Electric and Magnetic Source Imaging: A Systematic Review and Meta-Analysis. Front Neurol. 2019;10:1250.

4. Mouthaan B, Rados M, Boon P et al. Diagnostic accuracy of interictal source imaging in presurgical epilepsy evaluation: A systematic review from the E-PILEPSY consortium. *Clinical Neurophysiology*. 2019;130(5):845-855.

5. Gross J, Junghöfer M, Wolters C. Bioelectromagnetism in Human Brain Research: New Applications, New Questions. *The Neuroscientist*. 2021:107385842110547.

6. Oliva M, Meckes-Ferber S, Roten A, Desmond P, Hicks R, O'Brien T. EEG dipole source localization of interictal spikes in non-lesional TLE with and without hippocampal sclerosis. *Epilepsy Res*. 2010;92(2-3):183-190.

7. Kargiotis O, Lascano A, Garibotto V et al. Localization of the epileptogenic tuber with electric source imaging in patients with tuberous sclerosis. *Epilepsy Res*. 2014;108(2):267-279.

8. Aydin Ü, Rampp S, Wollbrink A et al. Zoomed MRI Guided by Combined EEG/MEG Source Analysis: A Multimodal Approach for Optimizing Presurgical Epilepsy Work-up and its Application in a Multi-focal Epilepsy Patient Case Study. *Brain Topogr*. 2017;30(4):417-433.

9. Brodbeck V, Spinelli L, Lascano AM, et al. Electrical source imaging for presurgical focus localization in epilepsy patients with normal MRI. *Epilepsia*. 2010;51(4):583-591.

10. Lascano A, Perneger T, Vulliemoz S et al. Yield of MRI, high-density electric source imaging (HD-ESI), SPECT and PET in epilepsy surgery candidates. *Clinical Neurophysiology*. 2016;127(1):150-155.

11. Foged M, Martens T, Pinborg L et al. Diagnostic added value of electrical source imaging in presurgical evaluation of patients with epilepsy: A prospective study. *Clinical Neurophysiology*. 2020;131(1):324-329.

12. Dien J, Spencer K, Donchin E. Localization of the event-related potential novelty response as defined by principal components analysis. *Cognitive Brain Research*. 2003;17(3):637-650.

13. Wong T, Fung P, McAlonan G, Chua S. Spatiotemporal dipole source localization of face processing ERPs in adolescents: a preliminary study. *Behavioral and Brain Functions*. 2009;5(1):16.

14. Nemtsas P, Birot G, Pittau F et al. Source localization of ictal epileptic activity based on high-density scalp EEG data. *Epilepsia*. 2017;58(6):1027-1036.

15. Song J, Davey C, Poulsen C et al. EEG source localization: Sensor density and head surface coverage. *J Neurosci Methods*. 2015;256:9-21.

16. Seeck M, Koessler L, Bast T et al. The standardized EEG electrode array of the IFCN. *Clinical Neurophysiology*. 2017;128(10):2070-2077.

17. Lee S, Wu S, Tao JX, et al. Manifestation of Hippocampal Interictal Discharges on Clinical Scalp EEG Recordings. *J Clin Neurophysiol*. 2021;10.1097/WNP.0000000000000867.

18. Birot G, Spinelli L, Vulliémoz S, et al. Head model and electrical source imaging: a study of 38 epileptic patients. *Neuroimage Clin*. 2014;5:77-83.

19. Vorwerk J, Cho JH, Rampp S, Hamer H, Knösche TR, Wolters CH. A guideline for head volume conductor modeling in EEG and MEG. *Neuroimage*. 2014;100:590-607.

20. Montes-Restrepo V, van Mierlo P, Strobbe G, Staelens S, Vandenberghe S, Hallez H. Influence of skull modeling approaches on EEG source localization. *Brain Topogr*. 2014;27(1):95-111.

21. Azizollahi H, Aarabi A, Wallois F. Effects of uncertainty in head tissue conductivity and complexity on EEG forward modeling in neonates. *Hum Brain Mapp*. 2016;37(10):3604-3622.

22. Akalin Acar Z, Acar CE, Makeig S. Simultaneous head tissue conductivity and EEG source location estimation. *Neuroimage*. 2016;124(Pt A):168-180.

23. Vorwerk J, Aydin Ü, Wolters CH, Butson CR. Influence of Head Tissue Conductivity Uncertainties on EEG Dipole Reconstruction. *Front Neurosci*. 2019;13:531.

24. Beniczky S, Rosenzweig I, Scherg M, et al. Ictal EEG source imaging in presurgical evaluation: High agreement between analysis methods. *Seizure*. 2016;43:1-5.

25. Baroumand AG, Arbune AA, Strobbe G, et al. Automated ictal EEG source imaging: A retrospective, blinded clinical validation study. *Clin Neurophysiol*. 2021;S1388-2457(21)00530-7.

26. Aydin Ü, Vorwerk J, Dümpelmann M, et al. Combined EEG/MEG can outperform single modality EEG or MEG source reconstruction in presurgical epilepsy diagnosis. *PLoS One*. 2015;10(3):e0118753.

27. Mălîia MD, Meritam P, Scherg M, et al. Epileptiform discharge propagation: Analyzing spikes from the onset to the peak. *Clin Neurophysiol*. 2016;127(4):2127-2133.

28. McCann H, Pisano G, Beltrachini L. Variation in Reported Human Head Tissue Electrical Conductivity Values. *Brain Topogr*. 2019;32(5):825-858.

29. Antonakakis M, Schrader S, Aydin Ü, et al. Inter-Subject Variability of Skull Conductivity and Thickness in Calibrated Realistic Head Models. *Neuroimage*. 2020;223:117353.

30. Mégevand P, Spinelli L, Genetti M, et al. Electric source imaging of interictal activity accurately localises the seizure onset zone. *J Neurol Neurosurg Psychiatry*. 2014;85(1):38-43.

31. Park CJ, Seo JH, Kim D, et al. EEG Source Imaging in Partial Epilepsy in Comparison with Presurgical Evaluation and Magnetoencephalography. *J Clin Neurol*. 2015;11(4):319-330.

32. Russo A, Lallas M, Jayakar P, et al. The diagnostic utility of 3D-ESI rotating and moving dipole methodology in the pre-surgical evaluation of MRI-negative childhood epilepsy due to focal cortical dysplasia. *Epilepsia*. 2016;57(9):1450-1457.

33. Rikir E, Maillard LG, Abdallah C, et al. Respective Contribution of Ictal and Inter-ictal Electrical Source Imaging to Epileptogenic Zone Localization. *Brain Topogr*. 2020;33(3):384-402.

34. Urriola J, Bollmann S, Tremayne F, Burianová H, Marstaller L, Reutens D. Functional connectivity of the irritative zone identified by electrical source imaging, and EEG-correlated fMRI analyses. *Neuroimage Clin*. 2020;28:102440.

35. Heers M, Chowdhury RA, Hedrich T, et al. Localization Accuracy of Distributed Inverse Solutions for Electric and Magnetic Source Imaging of Interictal Epileptic Discharges in Patients with Focal Epilepsy. *Brain Topogr*. 2016;29(1):162-181.

36. Tamilia E, AlHilani M, Tanaka N, et al. Assessing the localization accuracy and clinical utility of electric and magnetic source imaging in children with epilepsy. *Clin Neurophysiol*. 2019;130(4):491-504.

37. Tao JX, Ray A, Hawes-Ebersole S, Ebersole JS. Intracranial EEG substrates of scalp EEG interictal spikes. *Epilepsia*. 2005;46(5):669-676.

38. Tao JX, Baldwin M, Ray A, Hawes-Ebersole S, Ebersole JS. The impact of cerebral source area and synchrony on recording scalp electroencephalography ictal patterns. *Epilepsia*. 2007;48(11):2167-2176.

39. Barborica A, Mindruta I, Sheybani L, et al. Extracting seizure onset from surface EEG with independent component analysis: Insights from simultaneous scalp and intracerebral EEG. *Neuroimage Clin*. 2021;32:102838.

40. Cox BC, Danoun OA, Lundstrom BN, Lagerlund TD, Wong-Kisiel LC, Brinkmann BH. EEG source imaging concordance with intracranial EEG and epileptologist review in focal epilepsy. *Brain Commun*. 2021;3(4):fcab278.

41. Parvizi J, Kastner S. Promises and limitations of human intracranial electroencephalography. *Nat Neurosci*. 2018;21(4):474-483.

42. Cuello Oderiz C, von Ellenrieder N, Dubeau F, et al. Association of Cortical Stimulation-Induced Seizure With Surgical Outcome in Patients With Focal Drug-Resistant Epilepsy. *JAMA Neurol*. 2019;76(9):1070-1078.

43. Sommer B, Rampp S, Doerfler A, et al. Investigation of subdural electrode displacement in invasive epilepsy surgery workup using neuronavigation and intraoperative MRI. *Neurol Res*. 2018;40(10):811-821.

44. Cuffin BN, Cohen D, Yunokuchi K, et al. Tests of EEG localization accuracy using implanted sources in the human brain. *Ann Neurol*. 1991;29(2):132-138.

45. Krings T, Chiappa KH, Cuffin BN, Cochius JI, Connolly S, Cosgrove GR. Accuracy of EEG dipole source localization using implanted sources in the human brain. *Clin Neurophysiol*. 1999;110(1):106-114.

46. Roth BJ, Balish M, Gorbach A, Sato S. How well does a three-sphere model predict positions of dipoles in a realistically shaped head?. *Electroencephalogr Clin Neurophysiol*. 1993;87(4):175-184.

47. Yvert B, Bertrand O, Echallier JF, Pernier J. Improved dipole localization using local mesh refinement of realistic head geometries: an EEG simulation study. *Electroencephalogr Clin Neurophysiol*. 1996;99(1):79-89.

48. Whittingstall K, Stroink G, Gates L, Connolly JF, Finley A. Effects of dipole position, orientation and noise on the accuracy of EEG source localization. *Biomed Eng Online*. 2003;2:14. Published 2003 Jun 6.

49. Mikulan E, Russo S, Parmigiani S, et al. Simultaneous human intracerebral stimulation and HD-EEG, ground-truth for source localization methods. *Sci Data*. 2020;7(1):127. Published 2020 Apr 28.

50. Vanrumste B, Van Hoey G, Van de Walle R, D'Havé M, Lemahieu I, Boon P. Dipole location errors in electroencephalogram source analysis due to volume conductor model errors. *Med Biol Eng Comput*. 2000;38(5):528-534.

51. Laarne PH, Tenhunen-Eskelinen ML, Hyttinen JK, Eskola HJ. Effect of EEG electrode density on dipole localization accuracy using two realistically shaped skull resistivity models. *Brain Topogr*. 2000;12(4):249-254.

52. Chen F, Hallez H, Staelens S. Influence of skull conductivity perturbations on EEG dipole source analysis. *Med Phys*. 2010;37(8):4475-4484.

53. Wang G, Yang L, Worrell G, He B. The relationship between conductivity uncertainties and EEG source localization accuracy. *Annu Int Conf IEEE Eng Med Biol Soc*. 2009;2009:4799-4802.

54. Pohlmeier R, Buchner H, Knoll G, Rienäcker A, Beckmann R, Pesch J. The influence of skull-conductivity misspecification on inverse source localization in realistically shaped finite element head models. *Brain Topogr*. 1997;9(3):157-162.

55. Rimpiläinen V, Koulouri A, Lucka F, Kaipio JP, Wolters CH. Improved EEG source localization with Bayesian uncertainty modelling of unknown skull conductivity. *Neuroimage*. 2019;188:252-260.

56. Oostendorp TF, Delbeke J, Stegeman DF. The conductivity of the human skull: results of in vivo and in vitro measurements. *IEEE Trans Biomed Eng*. 2000;47(11):1487-1492.

57. Lucka F, Pursiainen S, Burger M, Wolters CH. Hierarchical Bayesian inference for the EEG inverse problem using realistic FE head models: depth localization and source separation for focal primary currents. *Neuroimage*. 2012;61(4):1364-1382.

58. Haueisen J, Ramon C, Eiselt M, Brauer H, Nowak H. Influence of tissue resistivities on neuromagnetic fields and electric potentials studied with a finite element model of the head. *IEEE Trans Biomed Eng*. 1997;44(8):727-735.

59. Haueisen J, Böttner A, Nowak H, Brauer H, Weiller C. The influence of conductivity changes in boundary element compartments on the forward and inverse problem in electroencephalography and magnetoencephalography. *Biomed Tech (Berl)*. 1999;44(6):150-157.

60. Jazbinšek V, Hren R. Influence of randomly displaced BSPM leads on the identification of ventricular preexcitation sites. Biomed Tech (Berl). 1999;44 (Suppl 2):S104-107.

61. Haueisen J, Tuch DS, Ramon C, et al. The influence of brain tissue anisotropy on human EEG and MEG. *Neuroimage*. 2002;15(1):159-166.

62. Wolters CH, Anwander A, Tricoche X, Weinstein D, Koch MA, MacLeod RS. Influence of tissue conductivity anisotropy on EEG/MEG field and return current computation in a realistic head model: a simulation and visualization study using high-resolution finite element modeling. *Neuroimage*. 2006;30(3):813-826.

63. Hallez H, Vanrumste B, Van Hese P, Delputte S, Lemahieu I. Dipole estimation errors due to differences in modeling anisotropic conductivities in realistic head models for EEG source analysis. *Phys Med Biol*. 2008;53(7):1877-1894.

64. Güllmar D, Haueisen J, Reichenbach JR. Influence of anisotropic electrical conductivity in white matter tissue on the EEG/MEG forward and inverse solution. A high-resolution whole head simulation study. *Neuroimage*. 2010;51(1):145-163.

65. Haueisen J, Ramon C, Brauer H, Nowak H. The influence of local tissue conductivity changes on the magnetoencephalogram and the electroencephalogram. *Biomed Tech (Berl)*. 2000;45(7-8):211-214.

66. Ramon C, Schimpf P, Haueisen J, Holmes M, Ishimaru A. Role of soft bone, CSF and gray matter in EEG simulations. *Brain Topogr*. 2004;16(4):245-248.

67. Koessler L, Colnat-Coulbois S, Cecchin T, Hofmanis J, Dmochowski JP, Norcia AM. et al. In-vivo measurements of human brain tissue conductivity using focal electrical current injection through intracerebral multicontact electrodes. *Hum Brain Mapp*. 2017;38(2):974-986.

68. Ramon C, Garguilo P, Fridgeirsson EA, Haueisen J. Changes in scalp potentials and spatial smoothing effects of inclusion of dura layer in human head models for EEG simulations. *Front Neuroeng*. 2014;7:32.

69. Fiederer LDJ, Vorwerk J, Lucka F, et al. The role of blood vessels in high-resolution volume conductor head modeling of EEG. *Neuroimage*. 2016;128:193-208.

70. Ollikainen JO, Vauhkonen M, Karjalainen PA, Kaipio JP. Effects of local skull inhomogeneities on EEG source estimation. *Med Eng Phys*. 1999;21(3):143-154.

71. Lanfer B, Scherg M, Dannhauer M, Knösche TR, Burger M, Wolters CH. Influences of skull segmentation inaccuracies on EEG source analysis. *Neuroimage*. 2012;62(1):418-431.

72. Lillie EM, Urban JE, Lynch SK, Weaver AA, Stitzel JD. Evaluation of Skull Cortical Thickness Changes With Age and Sex From Computed Tomography Scans. *J Bone Miner Res*. 2016;31(2):299-307.

73. Tang C, You F, Cheng G, et al. Correlation between structure and resistivity variations of the live human skull. *IEEE Trans Biomed Eng*. 2008;55(9):2286-2292.

74. Hori H, Moretti G, Rebora A, Crovato F. The thickness of human scalp: normal and bald. *J Invest Dermatol*. 1972;58(6):396-399.

75. Cuffin BN. Effects of local variations in skull and scalp thickness on EEG's and MEG's. *IEEE Trans Biomed Eng*. 1993;40(1):42-48.

76. Chauveau N, Franceries X, Doyon B, Rigaud B, Morucci JP, Celsis P. Effects of skull thickness, anisotropy, and inhomogeneity on forward EEG/ERP computations using a spherical three-dimensional resistor mesh model. *Hum Brain Mapp*. 2004;21(2):86-97.

77. Rice JK, Rorden C, Little JS, Parra LC. Subject position affects EEG magnitudes. *Neuroimage*. 2013;64:476-484.

78. Mosher JC, Spencer ME, Leahy RM, Lewis PS. Error bounds for EEG and MEG dipole source localization. *Electroencephalogr Clin Neurophysiol*. 1993;86(5):303-321.

79. Yvert B, Bertrand O, Thévenet M, Echallier JF, Pernier J. A systematic evaluation of the spherical model accuracy in EEG dipole localization. *Electroencephalogr Clin Neurophysiol*. 1997;102(5):452-459.

80. Lantz G, Grave de Peralta R, Spinelli L, Seeck M, Michel CM. Epileptic source localization with high density EEG: how many electrodes are needed?. *Clin Neurophysiol*. 2003;114(1):63-69.

81. Michel CM, Lantz G, Spinelli L, De Peralta RG, Landis T, Seeck M. 128-channel EEG source imaging in epilepsy: clinical yield and localization precision. *J Clin Neurophysiol*. 2004;21(2):71-83.

82. Rikir E, Koessler L, Gavaret M, et al. Electrical source imaging in cortical malformation-related epilepsy: a prospective EEG-SEEG concordance study. *Epilepsia*. 2014;55(6):918-932.

83. Akhtari M, Bryant HC, Mamelak AN, et al. Conductivities of three-layer live human skull. *Brain Topogr*. 2002;14(3):151-167.

84. Dannhauer M, Lanfer B, Wolters CH, Knösche TR. Modeling of the human skull in EEG source analysis. *Hum Brain Mapp*. 2011;32(9):1383-1399.

85. von Ellenrieder N, Beltrachini L, Muravchik CH. Electrode and brain modeling in stereo-EEG. *Clin Neurophysiol*. 2012;123(9):1745-1754.

86. Medani T, Lautru D, Schwartz D, Ren Z, Sou G. FEM Method for the EEG Forward Problem and Improvement Based on Modification of the Saint Venant's Method. *Progress In Electromagnetics Research*. 2015;153:11-22.

87. Zelmann R, Lina JM, Schulze-Bonhage A, Gotman J, Jacobs J. Scalp EEG is not a blur: it can see high frequency oscillations although their generators are small. *Brain Topogr*. 2014;27(5):683-704.

88. Plonsey R, Heppner DB. Considerations of quasi-stationarity in electrophysiological systems. *Bull Math Biophys*. 1967;29(4):657-664.

89. Grave de Peralta Menendez R, Gonzalez Andino S. Electrical Neuroimaging with Irrotational Sources. *Comput Math Methods Med*. 2015;2015:801037.

90. Vorwerk J, Hanrath A, Wolters CH, Grasedyck L. The multipole approach for EEG forward modeling using the finite element method. *Neuroimage*. 2019;201:116039.

Figure legends

Figure 1 Steps of the workflow. (**A**) Scalp EEG channel over plot and topography map of the averaged stimulation potential was checked. (**B**) The individual pre-implantation MRI was segmented and scalp electrode data on the post-implantation CT were co-registered to the MRI to generate the individual FEM head model. Eleven skull conductivity values were applied to the individual FEM head model. (**C**) The locations of scalp and stereo-EEG contacts were identified on the post-implantation CT and the CT-dataset was co-registered to pre-implantation MRI. Talairach co-ordinates of contacts were extracted from the MRI. (**D**) ESI of the averaged stimulation potential was performed using an individual FEM model. (**E**) Lastly, Talairach co-ordinates of stereo-EEG contacts from step (**C)** and Talairach co-ordinates of the estimated dipole (red) from step (**D)** were used to analyze the localization error and the offset direction (yellow arrow). Remark: post-implantation MRI on figure (**D**) and (**E**) are for illustration purpose.

Figure 2 Relationship between localization error and goodness of fit. Density plot of all fitted dipoles with goodness of fit ≥80% on localization error (X-axis) against goodness of fit (Y-axis).

Figure 3 Relationships between source depth and localization error. (**A**) Density plot of dipoles on source depth (X-axis) against localization error (Y-axis) across all skull: scalp conductivity ratios (SSCR). (**B-L**) Scatter plots of dipoles on source depth (X-axis) against localization errors (Y-axis) in 11 SSCR (1:8 to1:330, separate figures). (**B-C**) Based on Pearson correlation, source depth and localization error were moderately correlated, r (324) = [0.55], P = 0.000 for SSCR 1:330 and r (325) = [0.49], P = 0.000 for SSCR 1:165. (**D-J**) For other SSCR, source depth and localization error were weakly correlated, r (325) = [0.38], P =

0.000 for SSCR 1:80 and 1:70, r (332) = [0.34], P = 0.000 for SSCR 1:55, r (326) = [0.26], P = 0.000 for SSCR 1:41, r (326) = [0.14], P = 0.01 for SSCR 1:33, r (326) = [0.11], P = 0.06 for SSCR 1:28, r (327) = [0.01], P = 0.86 for SSCR 1:24. (**K &L**) For SSCR 1:16 and 1:8, source depth and localization error were weakly inversely correlated, r (328) = [-0.18], P = 0.001 and r (333) = [-0.42], P = 0.000 respectively.

Figure 4 Relationships between skull: scalp conductivity ratio (SSCR) and localization error. (**A**) Box plot of localization errors (Y-axis) in relation to SSCR (X-axis) showing median localization errors and interquartile ranges across all source depths. (**B-F**) Box plots of localization errors in relation to SSCR in different source depth ranges. Red crosses mark mean localization errors. *, **, *** are marked at SSCR 1:80, 1:16, and 1:8 respectively. (**B-C**) Based on Pearson correlation, SSCR and localization error were not correlated, r (350) = [0.08], P = 0.16 for source depth ≤10 mm and r (716) = [0.06], P = 0.09 for source depth >10-20 mm. (**D-F**) For other depth ranges, SSCR and localization error were inverse correlated, r (1,095) = [-0.2], P = 0.000 for source depth >20-30 mm, r (1,002) = [-0.53], P = 0.000) for source depth >30-40 mm and r (446) = [-0.58], P = 0.000 for source depth >40 mm.

Figure 5 The offset direction of estimated dipoles. Diagram showing number of dipoles (Y-axis) on each category offset direction (block pattern) for all source depth ranges (each compartment) across all scalp: skull conductivity ratios (SSCR, X-axis).

Figure 6 The offset direction of estimated dipoles in different anatomy locations using standard adult skull conductivity (SSCR 1:80). (**A-C**) The offset direction of the estimated dipole (red) with source located in mesial temporal structure shifted outward-forward-downward, in relation to location of stimulating contacts (crosshair). (**D-F**) The offset direction of the estimated dipole (red) with source located in lateral temporal cortex shifted inward-forward-downward in relation to location of stimulating contacts (crosshair). (**G-I**) The offset direction of the estimated dipole (red) with source located in lateral frontal cortex shifted inward-forward-downward in relation to location of stimulating contacts (crosshair). Remark: post-implantation MRI on the figures are for illustration purpose.

Table1 Mean localization error and standard deviation (mm), observed from sources located in different depths, tissues and anatomical regions, using 11 skull: scalp conductivity ratios (SSCR).

SSCR	*1:8*	*1:16*	*1:24*	*1:28*	*1:33*	*1:41*	*1:55*	*1:70*	*1:80*	*1:165*	*1:330*
	n=335	n=330	n=329	n=328	n=328	n=328	n=334	n=327	n=327	n=327	n=326
Depth											
>40 mm (n=40-42)	10.7 ±4.4	12.8 ±4.6	15 ±4.4	17.3 ±5.4	17.7 ±5.1	19.7 ±5.5	21.9 ±6.1	22.6 ±6.2	23.4 ±6.4	25 ±7.1	26 ±5.9
>30-40 mm (n=91-93)	10.3 ±4.2	11 ±4.2	12.3 ±4.4	13.5 ±4.8	14.5 ±5	15.8 ±4.9	17.7 ±5.2	19 ±5.2	20.4 ±5.5	21.4 ±5.7	23.1 ±4.6
>20-30 mm (n=99-102)	13.3 ±5	12.5 ±5.1	12.8 ±5.2	12.8 ±5.4	12.8 ±5.6	13.6 ±5.9	14.9 ±6.4	15.5 ±6.2	16.8 ±6.9	16.9 ±6.5	19.1 ±5.6
>10-20 mm (n=64-66)	16.8 ±7	15.1 ±6.9	14 ±6.4	14.1 ±6.8	14.4 ±6.4	14.2 ±6.2	14.6 ±6.4	14.7 ±6.3	15.8 ±7.2	14.7 ±6.4	15.7 ±5.9
≤10 mm (n=32)	16.6 ±6.2	13.8 ±6.9	12.8 ±6.9	13.3 ±7.1	13.9 ±7	13.6 ±6.2	14 ±7	14.4 ±6.9	14.4 ±7	13.7 ±7.3	15 ±5.7
All depths	13.2 ±5.9	12.8 ±5.6	13.2 ±5.4	13.9 ±5.9	14.3 ±5.8	15.1 ±6	16.4 ±6.6	17.1 ±6.6	18.2 ±7.1	18.4 ±7.3	20 ±6.5
Tissue											
Deep grey (n=68-70)	11.5 ±4.8	13 ±5.1	14.6 ±5.2	16.2 ±6.1	16.9 ±5.9	18.7 ±6.3	20.6 ±6.6	21.4 ±6.8	22.1 ±7	23.5 ±7.4	24.6 ±5.7
White (n=65)	12.4 ±6.4	12.3 ±6.1	12.7 ±5.3	13.8 ±6.3	13.7 ±5.8	14.4 ±5.5	16 ±5.8	16.8 ±6	18.1 ±6.5	18.9 ±6.2	21.1 ±5.4
White- grey (n=92-93)	12.4 ±6.4	12 ±5.1	12.6 ±4.8	12.9 ±4.5	13.4 ±4.8	14.2 ±5	15 ±5.3	16.3 ±6.4	17.7 ±6.1	17.7 ±5.7	19.3 ±5
Superficial grey (n=90-92)	16.1 ±6	14.1 ±5.9	13.3 ±5.8	13.3 ±6.1	13.8 ±6.1	13.9 ±6.2	14.4 ±6.3	14.5 ±6.4	15.6 ±7.3	14.8 ±7.1	16 ±6.8
CSF (n=11-15)	10.8 ±4.3	10 ±5.5	11.3 ±6.6	12.3 ±7.8	13.7 ±7.9	14 ±6.3	19.5 ±8.9	19.2 ±7.5	19.6 ±7.9	19.1 ±9.2	22.5 ±5.5
Anatomy											
Lateral temporal (n=50-52)	16.7 ±5.8	14.6 ±4.8	13.5 ±4.4	13.3 ±4.6	13.6 ±4.6	13.5 ±4.4	13.5 ±4.6	13.4 ±4.5	14.4 ±5	13.4 ±4.2	14.9 ±4.8
Mesial temporal (n=66-68)	11.2 ±4	12.9 ±4.3	14.7 ±4.4	16.4 ±5.5	17.1 ±5.2	18.8 ±5.5	20.9 ±5.6	21.8 ±5.9	22.5 ±6.1	24 ±6.6	25.1 ±5.3
Lateral frontal (n=39)	15.3 ±6.5	12.7 ±7.6	12 ±7.4	12.2 ±7.6	12.8 ±7.5	13.3 ±7.7	14 ±7.6	14 ±7.2	15.4 ±8.6	14.5 ±8	15.5 ±6.7
Mesial frontal (n=3)	21.5 ±3.9	22.6 ±4.9	25 ±4.9	25 ±4.9	27 ±5.6	29.5 ±5.8	30.9 ±4.6	33.3 ±4.6	34.7 ±4.5	36.8 ±3.1	36 ±2.2

Table 2 Studies evaluating the relationship between localization error and source depth

Study	*Method*	*Brain area*	*Scalp EEG*	*Number of trials*[a]	*Head model*	*Skull conductivity (S/m)*	*Inverse solution*	*Average localization error (mm)*	*Source depth (mm)*
Cuffin et al, 1991	electrical stimulation	frontal, temporal	21	12	spherical	0.0042	dipole	11	
Roth et al, 1993	simulation	frontal, temporal	21	8	BEM	0.0056		19.7	~ mesial temporal
Yvert et al, 1996	simulation	parietal, temporal	21	24	spherical, BEM	0.0056	dipole	2-3	>30
								4-6	≤30
Krings et al, 1999	electrical stimulation	temporal	21	10	spherical	0.0042	dipole	19.3/16.4	40-57/ 62-85
			41					8.9/17	40-57/ 62-85
Whittingstall et al, 2003	simulation	parietal, temporal	21	92	BEM	0.0042	dipole	35-65	35-70
								5-35	0-35
Mikulan et al, 2020	electrical stimulation	frontal, parietal, temporal	32-256	61	BEM	0.006	MNE	2-36	15-55
							dSPM	2-27	15-55
							eLORETA	2-21	15-55

[a]: number of stimulation locations or simulation dipoles

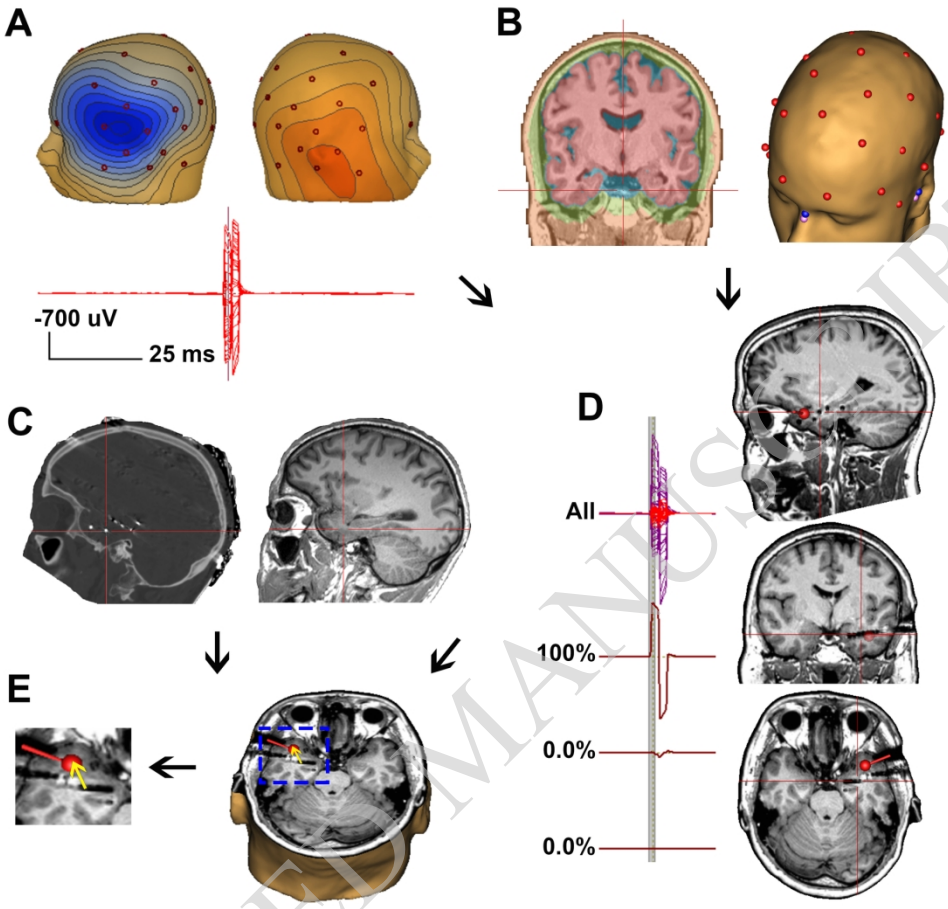

Figure 1

170x159mm (300 x 300 DPI)

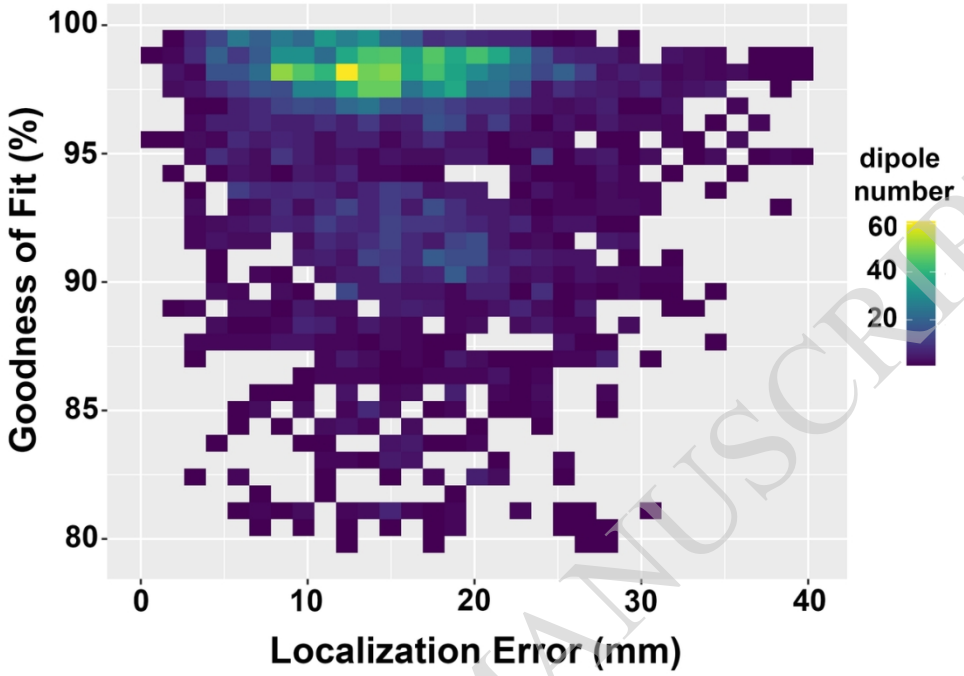

Figure 2

114x85mm (300 x 300 DPI)

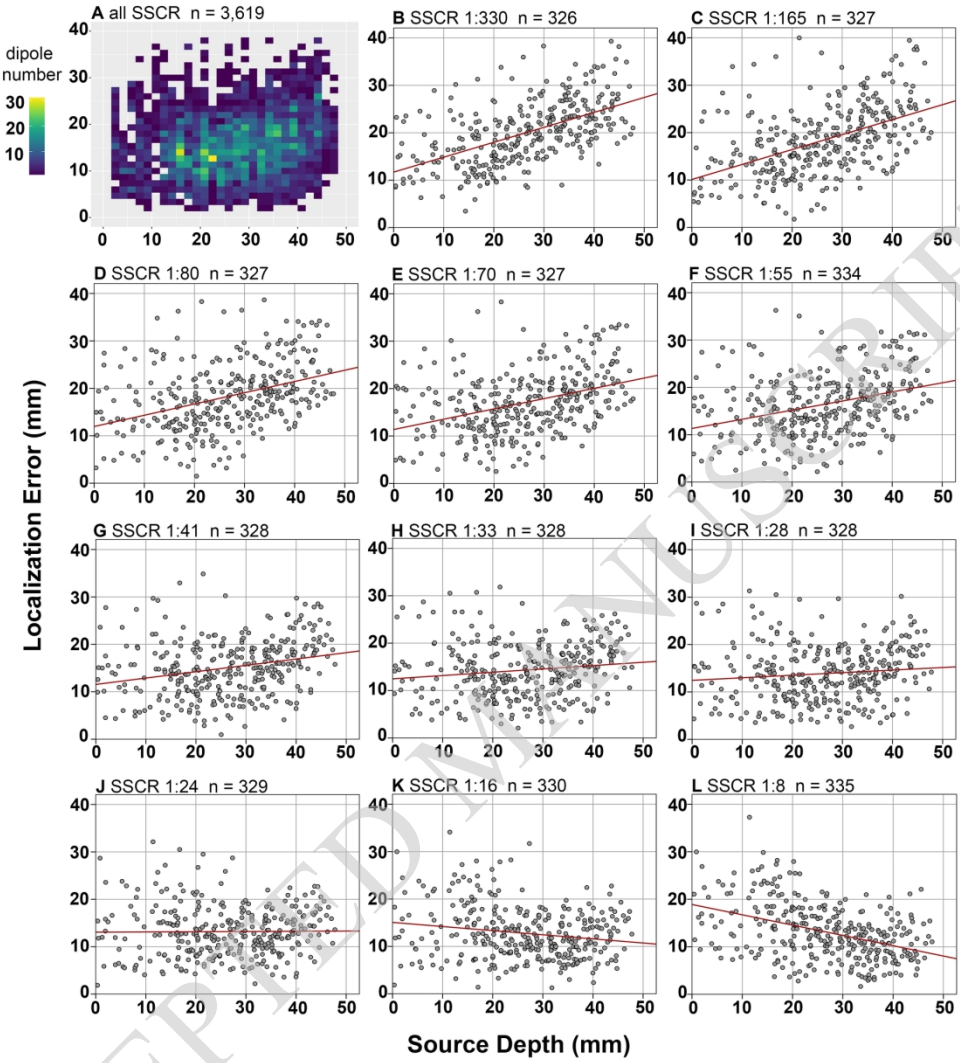

Figure 3

170x185mm (300 x 300 DPI)

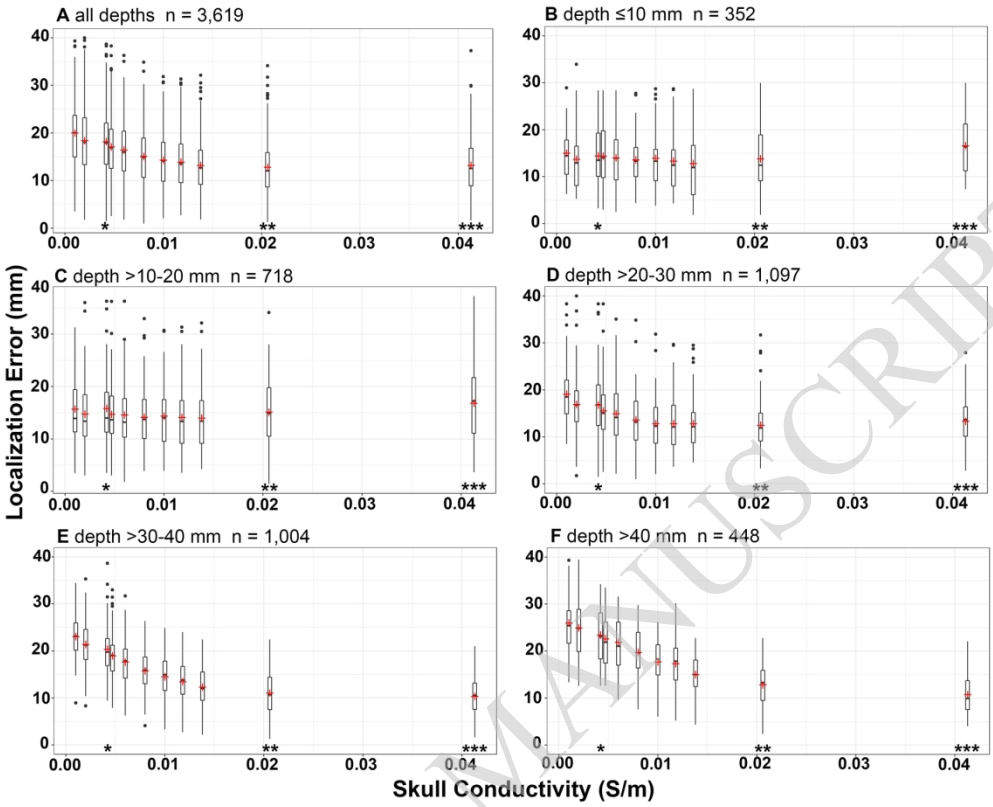

Figure 4

170x137mm (300 x 300 DPI)

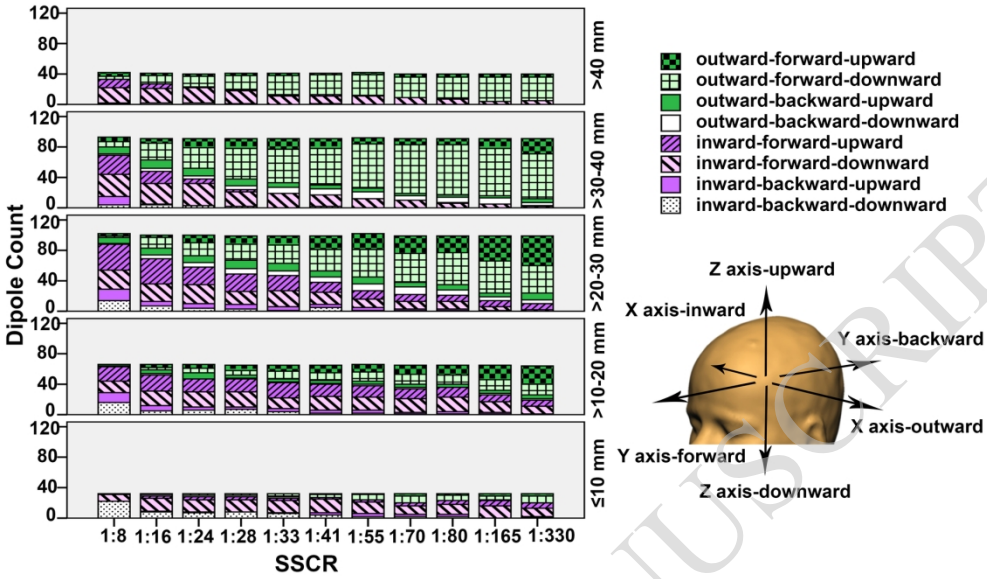

Figure 5

169x105mm (300 x 300 DPI)

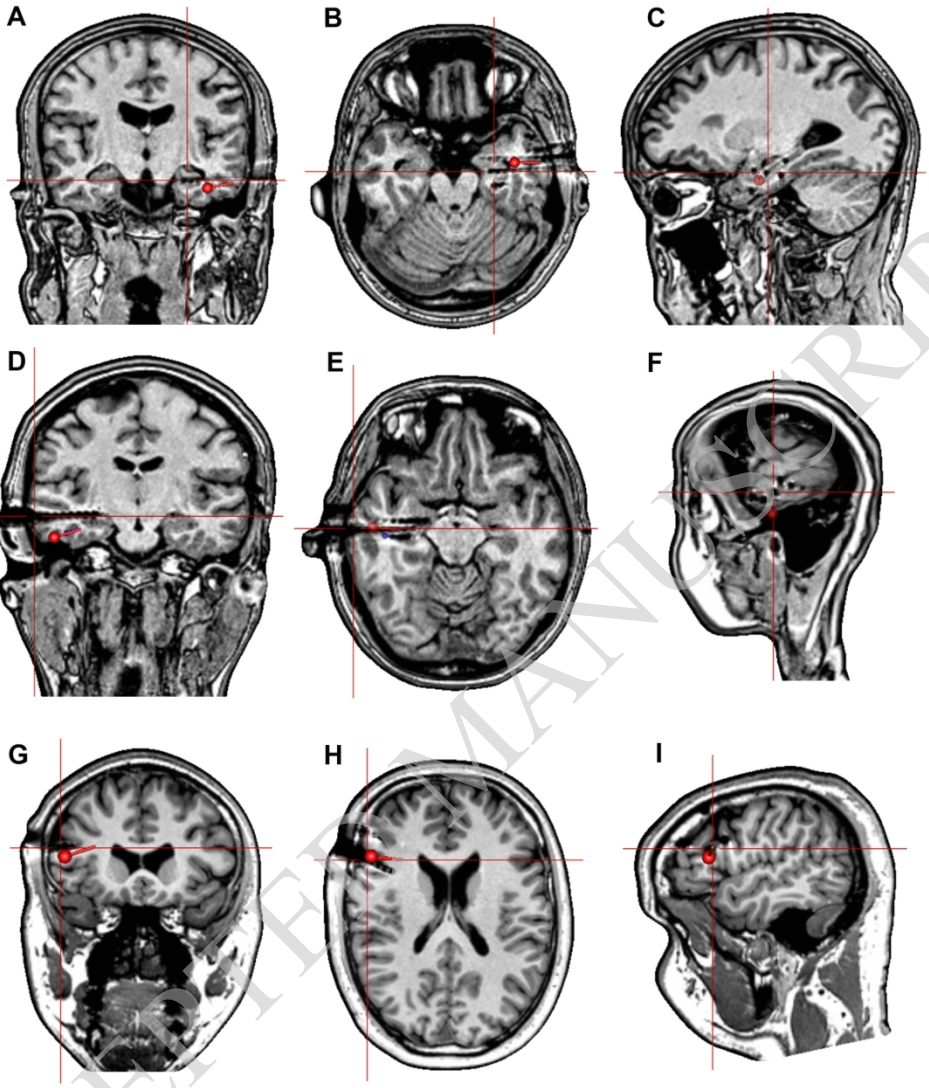

Figure 6

170x191mm (300 x 300 DPI)

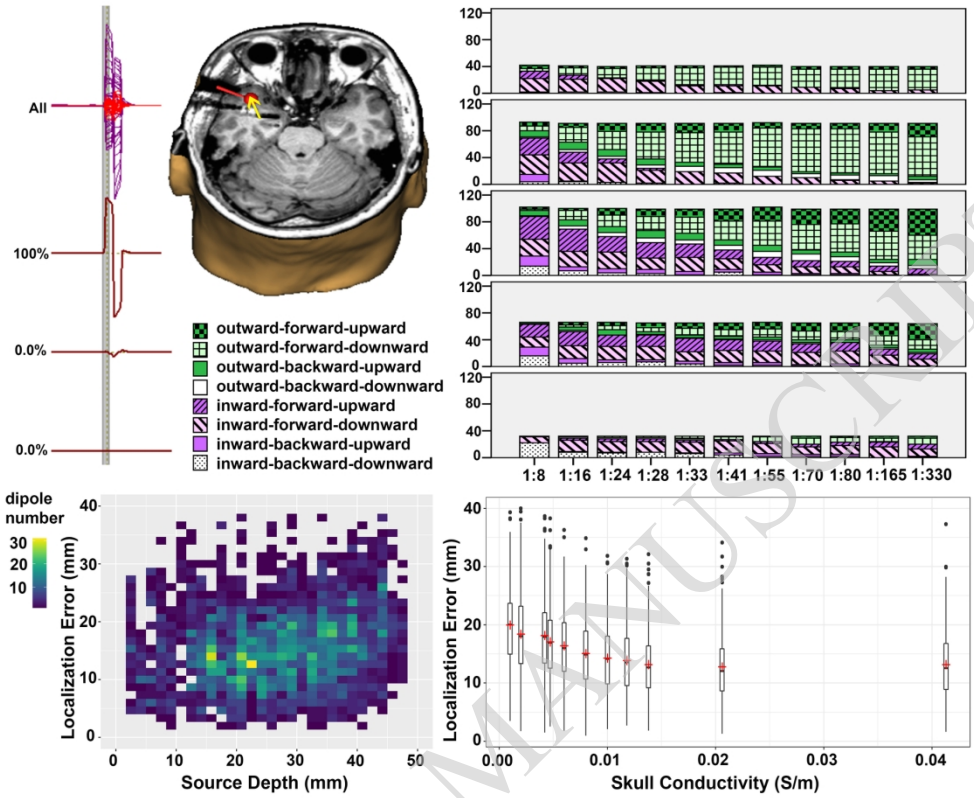

Graphical abstract

170x138mm (300 x 300 DPI)